RESEARCH ARTICLE | MARCH 01 2024

Time-reversible and fully time-resolved ultra-narrowband biphoton frequency combs

Kai-Chi Chang ; Xiang Cheng ; Murat Can Sarihan ; Chee Wei Wong

APL Quantum 1, 016106 (2024)
https://doi.org/10.1063/5.0180543

Time-reversible and fully time-resolved ultra-narrowband biphoton frequency combs

Cite as: APL Quantum 1, 016106 (2024); doi: 10.1063/5.0180543
Submitted: 10 October 2023 • Accepted: 15 December 2023 •
Published Online: 23 February 2024

Kai-Chi Chang,[a] Xiang Cheng,[b] Murat Can Sarihan, and Chee Wei Wong[c]

AFFILIATIONS

Fang Lu Mesoscopic Optics and Quantum Electronics Laboratory, Department of Electrical and Computer Engineering, University of California, Los Angeles, California 90095, USA

[a]Author to whom correspondence should be addressed: uclakcchang@g.ucla.edu
[b]chengxiang@g.ucla.edu
[c]cheewei.wong@g.ucla.edu

ABSTRACT

Time-reversibility, which is inherent in many physical systems, is crucial in tailoring temporal waveforms for optimum light–matter interactions. Among the time-reversible atomic systems, narrowband biphoton sources are essential for efficient quantum storage. In this work, we demonstrate time-reversed and fully time-resolved ultra-narrowband single-sided biphoton frequency combs with an average free-spectral range (FSR) of 42.66 MHz and an average linewidth of 4.60 MHz in the telecommunication band. We experimentally observe the fully time-resolved and reversible temporal oscillations by second-order cross correlation and joint temporal intensity measurements. The potential benefits of the time-reversed and fully time-resolved temporal oscillations from our source include enhancing the efficiency of quantum storage in atomic memories and maximizing the utilization of temporal information in multimode biphoton frequency combs. We further verify the heralded single-photon state generation from the multimode biphoton frequency combs by using Hanbury Brown and Twiss interference measurements. To the best of our knowledge, this 42.66 MHz FSR of our photon-pair source represents the narrowest among all of the different configurated biphoton sources reported to date. This ultra-narrow FSR and its 4.60 MHz linewidth provide the highest frequency mode number of 5786 and the longest coherence time among all the singly configurated biphoton sources so far. Our time-reversed and fully time-resolved massive-mode biphoton source could be useful for high-dimensional quantum information processing and efficient time–frequency multiplexed quantum storage toward long-distance and large-scale quantum networks.

I. INTRODUCTION

Time-reversibility has proven to be ubiquitous in various branches of physics, including classical[1–15] and quantum systems.[16–27] For example, time-reversal techniques were exploited to optimize the efficiency of storage and retrieval of photons in atomic ensembles[3,4,10,17,19] and coherent perfect absorbers,[8,14] to realize near-unity absorption efficiency using microwave photons[21–23] and photonic crystals,[7] and to realize superabsorption.[15] Furthermore, time-reversal techniques have found many applications, such as strong focusing,[5,9] holography,[12] transfer of quantum state between distant optical[18] and microwave cavities,[24] and quantum communication.[25] Among the time-reversible systems, the absorption of single photons by atomic ensembles is a fundamentally interesting problem and has important applications in quantum science because it forms the essential element of a quantum repeater, the quantum memories.[28,29] The standard atomic quantum memory protocols include electromagnetically induced transparency (EIT),[30,31] controlled reversible inhomogeneous broadening (CRIB),[32,33] gradient echo memory (GEM),[17] and atomic frequency comb (AFC).[34,35] It is known that the quantum sources have to be resonant with atoms and exhibit narrow spectra that match the bandwidth of these quantum memories (typically between 0.1 and 100 MHz).[28,29,36] Nevertheless, the typical bandwidth of spontaneous parametric downconversion (SPDC)[29,37] and spontaneous four-wave mixing[38] spans a range of 0.1 to 100 THz. There are several orders of magnitude difference between quantum source and atomic quantum memories.

An effective approach to address this challenge is to employ cavity-enhanced[26,39–57] or filtered schemes[58–62] to narrow the output spectrum of SPDC or through four-wave mixing on chip.[63–65] However, all previous SPDC and four-wave mixing sources have either lacked time-reversibility[39–42,44–47,50–60] or are not compatible with the bandwidth of atomic memories.[26,40–43,45,49,50,54,61,62] While the time-reversal waveforms of a singly resonant photon-pair source have been demonstrated,[26] the result only shows time-reversed waveforms of a single-frequency mode without multimode temporal oscillations.

In this study, we present the demonstration of a time-reversed, fully time-resolved, ultra-narrowband telecommunication biphoton source utilizing single-sided biphoton frequency combs (BFCs) across a massive number of over 5000 frequency modes. Our approach involves realizing reversing temporal oscillations in the biphoton source by a planar fiber Fabry–Pérot cavity (FFPC). This FFPC is effectively exchanged between the signal and idler channels within the single-sided BFCs. We directly observe fully time-resolved and time-reversed second-order cross correlation and joint temporal intensity (JTI) from our biphoton sources without any temporal broadening from the commercial single-photon detectors. The average measured cavity free-spectral range (FSR) and the linewidth of exponential-decay and time-reversed single-sided BFCs are ≈42.66 MHz, ≈4.60 MHz, ≈42.67 MHz, and ≈4.60 MHz, respectively. The time-reversibility and fully time-resolved temporal oscillations in our source can be useful for improving the quantum storage efficiency in atomic memories and completely utilizing the temporal information in multimode BFCs.

Subsequently, we conducted Hanbury Brown and Twiss (HBT) interference measurements to validate the generation of single photons using our time-reversed single-sided BFCs. We verified this for each cavity round trip, and we measured minimum heralded $g^{(2)}(0) = 0.013 \pm 0.002$ and $g^{(2)}(0) = 0.016 \pm 0.002$ for the zeroth round trip with our time-reversible singly filtered BFCs. The measured minimum heralded $g^{(2)}(0)$ for the first to fourth cavity round trips is all smaller than 0.5. We also observe minimum heralded $g^{(2)}(0) = 0.204 \pm 0.002$ and $g^{(2)}(0) = 0.212 \pm 0.002$ to further validate the multimode emission and preservation of single-photon generation in our source. Our biphoton source operates within the telecommunication band, and it exhibits the narrowest average cavity FSR of ≈42.66 MHz and linewidth of ≈4.60 MHz. Hence, our source is directly compatible with chip-scale AFC quantum memories[66,67] without conversion of quantum frequency.[68] By fully harnessing the potential of time-reversed single-sided BFCs in the frequency domain, our sources are expected to have an average number of 5786 and 5722 frequency modes, which can be useful for denser time–frequency quantum information processing and time–frequency multiplexed quantum storage toward long-distance quantum networks.

II. RESULTS

A. Theory and experimental setup

The biphotons generated from single-sided configurations have a well-defined time order.[26,69] Consequently, we begin with the two-photon wavefunction of the singly filtered BFC in the frequency domain, which can be approximated as

$$|\psi(\omega_S,\omega_I)\rangle = \sum_{m=-N}^{N} \int d\Omega\, f(\Omega - m\Delta\Omega)\,\mathrm{sinc}(A\Omega)\hat{a}_S^\dagger(\omega_S)\hat{a}_I^\dagger(\omega_I)|0\rangle, \tag{1}$$

where $\hat{a}_S^\dagger$ and $\hat{a}_I^\dagger$ are the creation operators for biphotons; ω_S and ω_I are the corresponding frequencies; the sinc function is the SPDC's phase-matching function with $A = 1.39/\pi B_{\mathrm{PM}}$, with $B_{\mathrm{PM}} \approx 247$ GHz being the full width at half maximum (FWHM) bandwidth of a type-II periodically poled KTiOPO4 (ppKTP) waveguide; $\Delta\Omega$ is the cavity FSR in rad s^{-1}; Ω is the detuning of the biphotons from their center frequency; $2N + 1$ is the number of cavity lines passed in the given bandwidth; and $f(\Omega - m\Delta\Omega)$ is the spectral amplitude of the mth cavity resonance, with $f(\Omega) = 1/[\Delta\omega + i\Omega]$. The expression for the temporal wavefunction of the exponential-decay singly filtered BFC can be given as follows:

$$\begin{aligned}|\psi_{exponential-decay}(t_S,t_I)\rangle = &\int_0^\infty d(t_I - t_S)\exp\left[\Delta\omega(t_S - t_I)\right]\\ &\times \sum_{m=-N}^{N}\mathrm{sinc}(Am\Delta\Omega)\cos\left[m\Delta\Omega(t_I - t_S)\right]\\ &\times \hat{a}_S^\dagger(t_S)\hat{a}_I^\dagger(t_I)|0\rangle,\end{aligned} \tag{2}$$

where we use $\Delta\Omega/2\pi \ll B_{\mathrm{PM}}$. The temporal behavior of the state exhibits periodic recurrences that align with the average round trip time of the cavity, $\Delta T = 2\pi/\Delta\Omega \approx 23.442$ ns. In this scenario, only the signal photons undergo filtering, resulting in the observation of exponential-decay waveforms. This is due to the higher probability of detecting the heralding idler photons before the filtered signal photons.

Meanwhile, we can reverse the temporal oscillations in a singly filtered BFC by switching a FFPC to the previously heralding channel. The temporal wavefunction of this time-reversed BFC can be expressed as

$$\begin{aligned}|\psi_{time-reversed}(t_S,t_I)\rangle = &\int_0^\infty d(t_I - t_S)\exp\left[\Delta\omega(t_I - t_S)\right]\\ &\times \sum_{m=-N}^{N}\mathrm{sinc}(Am\Delta\Omega)\cos\left[m\Delta\Omega(t_I - t_S)\right]\\ &\times \hat{a}_S^\dagger(t_S)\hat{a}_I^\dagger(t_I)|0\rangle.\end{aligned} \tag{3}$$

Here, only idler photons are filtered, while signal photons are for heralding. We can observe time-reversed waveform, and this behavior can be attributed to the increased likelihood of detecting the idler photons after the heralding signal photons have been detected. The corresponding formulas for JTIs of time-reversible singly filtered BFCs are given in the supplementary material.

To experimentally investigate this approach, we utilized the following experimental setup in Fig. 1(a). For the pumping source, we utilize an external cavity diode laser (ECDL) operating at a wavelength of 780 nm. The entangled photons are produced through a type-II ppKTP waveguide. To eliminate the residual pump photons, we employ a long-pass filter (LPF) and a bandpass filter (BPF) with a 95% passband transmission (specifically, the Semrock NIR01-1570/3 filter). The signal and idler photons are then separated using a polarizing beam splitter (PBS). To reverse the temporal oscillations of singly filtered BFCs, we selectively pass either the signal photons or the idler photons through a FFPC. Figure 1(b) displays

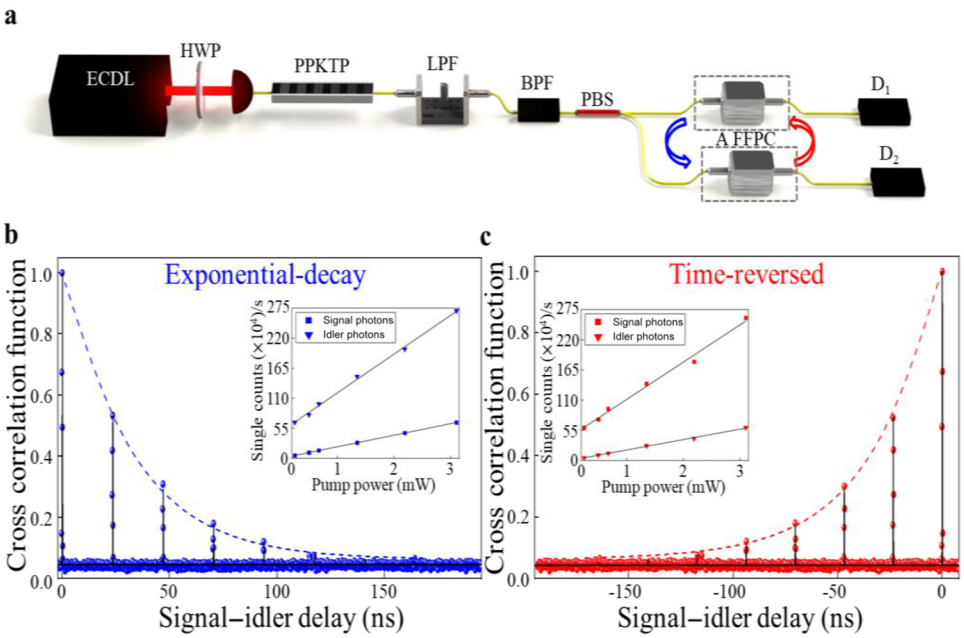

FIG. 1. Time-reversed ultra-narrowband biphoton source via single-sided BFCs. (a) Measurement setup for exponential-decay and time-reversed single-sided BFCs. ECDL: external cavity diode laser; HWP: half-wave plate; LPF: long-pass filter; BPF: bandpass filter; PBS: polarizing beam splitter; FFPC: fiber Fabry–Pérot cavity; and D: detector. (b) Fully time-resolved temporal waveforms of an exponential-decay single-sided BFC. For the exponential-decay single-sided BFC, the average cavity FSR is measured to be ≈23.442 ns or ≈42.66 MHz. The average cavity linewidth is measured to be ≈4.60 MHz, extracting from the theoretical fitting (black solid and dashed blue lines). The inset provides an example of the measured pump dependencies of single counts for signal photons and idler photons within the central correlation peak of the exponential-decay single-sided BFC. (c) Completely resolved temporal waveforms of a time-reversed single-sided BFC; its average cavity FSR is observed to be ≈23.438 ns or ≈42.67 MHz. The average cavity linewidth is measured to be ≈4.60 MHz, extracting from the theoretical fitting (black solid and red dashed lines). The inset provides an example of the measured pump dependencies of signal and idler counts in the central correlation peak of the time-reversed single-sided BFC. The ratio of the single counts remains similar for our time-reversible single-sided BFCs.

the fully time-resolved temporal waveforms of an exponential-decay single-sided BFC. For the exponential-decay single-sided BFC, the average cavity FSR is measured to be ≈23.442 ns, which is corresponding to ≈42.66 MHz. The average cavity linewidth is measured to be ≈4.60 MHz, deriving from the theoretical fitting (black solid and blue dashed lines). In Fig. 1(c), we present the completely resolved temporal waveforms of a time-reversed single-sided BFC; its average cavity FSR is measured to be ≈23.438 ns, which corresponds to ≈42.67 MHz. The cavity linewidth is measured to be ≈4.60 MHz, deriving from the theoretical fitting (black solid and red dashed lines). We note that the slight difference between the average cavity FSRs (≈42.66 and ≈42.67 MHz) for exponential-decay and time-reversed single-sided BFCs comes from the fitting error. We extract the average cavity FSR from measuring the temporal spacing between correlation peaks, which corresponds to the average of the spacing between every peak. Hence, here and throughout this work, we represent all our results with the average cavity FSR and linewidth, and the frequency mode number reported is calculated based on the average FWHM bandwidth of our SPDC source and the average cavity FSR. In Figs. 1(b) and 1(c), the inset illustrates the measured pump dependencies of single counts for signal and idler photons. The signal photons are represented by the blue symbols, while the red symbols represent the idler photons. These measurements were obtained from the central correlation peak in our time-reversible single-sided BFCs. In both single-sided BFCs, it is observed that the unfiltered idler (signal) photons exhibit higher single counts compared to the filtered signal (idler) photons. This discrepancy can be attributed to the filtering loss incurred by a FFPC. To ensure stable photon-counting measurements, we must regulate the temperature of the FFPC due to its ultra-narrow cavity FSR (corresponds to a cavity length of 2.04 m). Temperature control of the FFPC is performed through our custom-made double-temperature shielding layers, providing a temperature control stability of ~1.6 MHz (≈1 mK) over 24-h. Other detailed information of ultra-narrow FFPC used in this work is provided in the supplementary material.

B. Fully time-resolved and reversed photon statistics of single-sided biphoton frequency combs

Then, we proceed to measure the photon statistics of the exponential-decay single-sided BFC, as predicted in Eq. (2). The results of our measurements are presented in Fig. 2. It is important to note that in practical temporal measurements, the sharp peaks of the cross correlation function often appear broader or not resolvable due to the limited temporal resolution of the single-photon detectors.[26,39,40,42–54,58–61] In our study, we utilize a

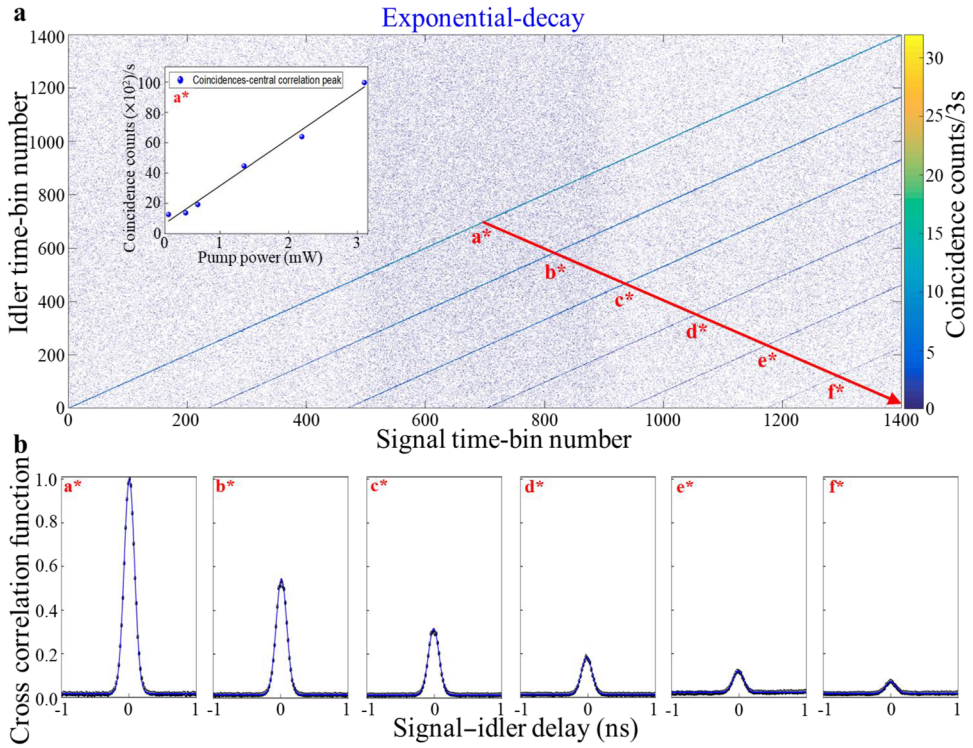

FIG. 2. Completely resolved joint temporal intensity and second-order cross correlation peaks in an exponential-decay single-sided BFC. (a) Completely resolved JTI in an exponential-decay single-sided BFC. The photon coincidence data are recorded between two detectors, and we sift the coincidence data into frames of duration $d \times T_{bin}$, comprised of d time-bins of duration T_{bin}. We choose T_{bin} to be 100 ps to enhance the resolution of temporal correlations. This d of 1400 shows that there are six clean cross correlations, from (a*) to (f*) in our ≈42.66 MHz single-sided BFC. The red arrow indicates both the cross sections of measured JTI [also shown in (b)] and the direction of single-sided temporal waveforms. The inset is the example pump dependencies of coincidence counts in the central correlation peak of the exponential-decay single-sided BFC. For the exponential-decay single-sided BFC, the coincidence counts exhibit a direct proportionality to the pump power. (b) Measured temporal second-order cross correlation oscillations from the cross sections of JTI in (a) for all six peaks. The normalized second-order cross correlation peak values are as follows: 1, 0.563, 0.349, 0.179, 0.121, and 0.075, respectively. Due to the ultra-narrow average cavity FSR of ≈42.66 MHz, the temporal correlation oscillations of the exponential-decay single-sided BFC can be fully time-resolved.

cavity with an average FSR of ≈42.66 MHz, enabling us to completely resolve the discretized JTI of the single-sided BFC without any temporal broadening. This result is performed using only commercial superconducting nanowire single-photon detectors (SNSPDs) with an approximate detection efficiency of 85% and a root-mean-square timing jitter of about 55 ps (Photon Spot, Inc.).

In Fig. 2(a), we record the coincidence counts of our exponential-decay single-sided BFC; then, we sift the coincidence data into frames of duration $d \times T_{bin}$, comprised of d time-bins of duration T_{bin}. We choose T_{bin} to be 100 ps to enhance the resolution of temporal correlations. This d of 1400 shows that there are six clean second-order cross correlation peaks, from (a^*) to (f^*) in our ≈42.66 MHz single-sided BFC. Each cross correlation peak represents the joint detection of biphotons corresponding to 0 to 5 cavity round trips. The red arrow indicates both the cross sections of measured JTI [also shown in Fig. 2(b)] and the direction of single-sided temporal waveforms. The inset of Fig. 2(a) is the example measured pump dependencies of coincidence counts from the central correlation peak in our exponential-decay singly filtered BFC. In Fig. 2(b), we show the measured temporal second-order cross correlation functions from the cross sections of JTI in Fig. 2(a). For Fig. 2(b), we normalize all the results with respect to the values of central correlation peak (a^*), whose peak value is measured to be 68.114. Then, the normalized second-order cross correlation peak values are as follows: 1, 0.563, 0.349, 0.179, 0.121, and 0.075, respectively. The FWHM of the six correlation peaks is consistent with the root-mean-square timing jitter of our commercial SNSPDs. This observation suggests that the JTI of our biphoton source is fully time-resolved. We want to emphasize that there are alternative approaches for achieving full resolution of the JTI in multimode biphoton sources. One such method is the utilization of ultrafast coincidence counting techniques,[70] time-lens,[71] or low-jitter SNSPDs.[72] These methods typically require either complex setups or specially designed SNSPDs.

In consistent with Eq. (3), in Fig. 3(a), we experimentally observe a time-reversed single-sided BFC, with six reversed second-order cross correlation peaks in the measured JTI. With its ≈42.67 MHz cavity FSR, we measure the fully time-resolved and reversed JTI via our single-sided BFC. The photon coincidence

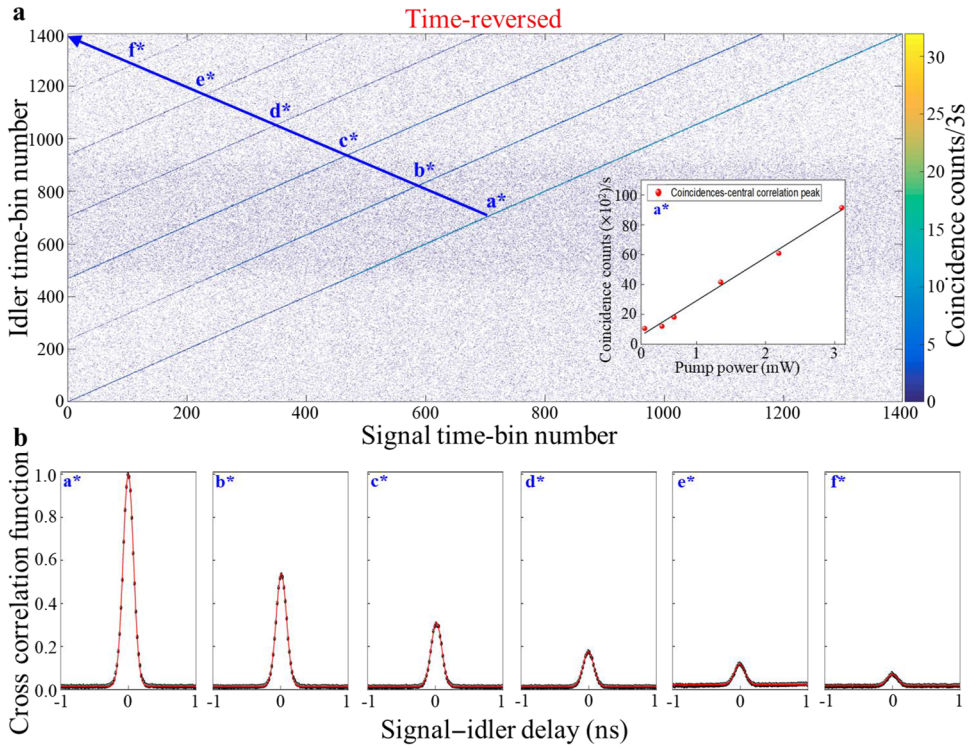

FIG. 3. Fully time-resolved joint temporal intensity and second-order cross correlation peaks in a reversing single-sided BFC. (a) Fully time-resolved JTI in a time-reversed single-sided BFC. The photon coincidence data are recorded between two detectors, and we sift the coincidence data into frames of duration $d \times T_{bin}$, comprised d time-bins of duration T_{bin}. We choose T_{bin} to be 100 ps to enhance the resolution of temporal correlations. This d of 1400 shows that there are six clean cross correlations, from (a*) to (f*) in our ≈42.67 MHz single-sided BFC. The blue arrow indicates both the cross sections of measured JTI [also shown in (b)] and the direction of single-sided temporal waveforms. We can clearly observe that the reverse of direction of single-sided temporal waveforms. The inset is the example pump dependencies of coincidence counts in the central correlation peak of the time-reversed single-sided BFC. In our time-reversed single-sided BFC, the coincidence counts exhibit a proportional relationship with the pump power. (b) Measured temporal second-order cross correlation oscillations from the cross sections of JTI in (a) for all six peaks. The normalized second-order cross correlation peak values are as follows: 1, 0.534, 0.320, 0.180, 0.120, and 0.076, respectively. Both the JTI and the temporal correlation oscillations of time-reversed single-sided BFC can be fully resolved owing to the ultra-narrow average cavity FSR of ≈42.67 MHz.

data are recorded and sifted into frames of duration $d \times T_{bin}$. To be consistent with measurements in Fig. 2, we choose T_{bin} to be 100 ps and the d be 1400, and we show that there are six clean cross correlation peaks, from (a*) to (f*) in our ≈42.67 MHz time-reversed single-sided BFC. The blue arrow indicates both the cross sections of measured JTI [also shown in Fig. 3(b)] and the direction of single-sided temporal waveforms. Interestingly, we can clearly observe the reversal in the direction of single-sided temporal oscillations, due to the asymmetric temporal waveform of the single-sided BFC. Our results in Figs. 1–3 are consistent with Eqs. (2) and (3). The inset of Fig. 3(a) is the example measured pump dependencies of coincidence counts from the central correlation peak in our time-reversed BFC. From Figs. 1–3, we measure and confirm that both the ratio of the single and coincidence counts is similar in our time-reversible singly filtered BFCs. Figure 3(b) shows the measured temporal second-order cross correlation functions from the cross sections of JTI in Fig. 3(a) for all six peaks. For Fig. 3(b), we normalize all the results with respect to the values of central correlation peak (a*), whose peak value is measured to be 73.420. Then, the normalized second-order cross correlation peak values are as follows: 1, 0.534, 0.320, 0.180, 0.120, and 0.076, respectively. In summary, in our time-reversible single-sided BFCs, the average cavity FSR ΔT is ≈23.438 ns and the average effective temporal resolution of SNSPDs T is ≈155.35 ps; therefore, we achieve an average ratio $T/\Delta T \approx 0.0066$, enabling us to experimentally fully resolve the JTI of our multimode biphoton sources using only commercial SNSPDs.

Next, we conducted measurements to examine the anti-bunching behavior of our time-reversed ultra-narrowband single-sided BFCs. In Fig. 4(a), we perform the HBT interference measurements via an exponential-decay singly filtered BFC. To access $g^{(2)}(0)$, we direct the idler photons to an HBT interferometer, heralded by the signal photons. The $g^{(2)}(0)$ value is measured from recording the threefold coincidence counts. Owing to the average cavity FSR (≈23.442 ns) and the FWHM of each cross correlation peak (average ≈155.6 ps), the accidental coincidence outside the correlated photons becomes dominant, leading to an increase in the value of $g^{(2)}(0)$. To address this, we adopt a coincidence window

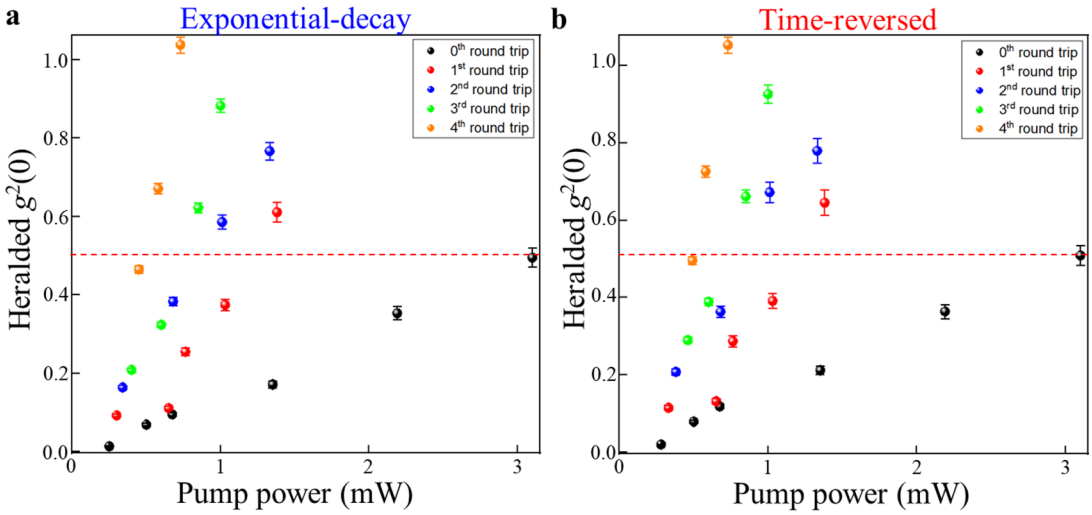

FIG. 4. Experimentally measured Hanbury Brown and Twiss interference of time-reversible ultra-narrowband single-sided BFCs. (a) The HBT measurements were conducted for our exponential-decay single-sided BFCs. The minimum heralded $g^{(2)}(0) = 0.013 \pm 0.002$ is obtained for the zeroth round trip at 0.25 mW pump power at a heralding rate of 20 kHz. For the first, second, third, and fourth cavity round trips, the minimum heralded $g^{(2)}(0)$ is extracted to be 0.092 ± 0.002, 0.164 ± 0.002, 0.208 ± 0.003, and 0.465 ± 0.003 with 0.3, 0.34, 0.4, and 0.45 mW, respectively. (b) HBT measurements using the time-reversed single-sided BFC. The minimum heralded $g^{(2)}(0) = 0.016 \pm 0.002$ is measured for the zeroth round trip at 0.28 mW pump power at a heralding rate of 24 kHz. For the first, second, third, and fourth cavity round trips, the minimum heralded $g^{(2)}(0)$ is measured to be 0.115 ± 0.002, 0.207 ± 0.002, 0.247 ± 0.003, and 0.496 ± 0.003 with 0.33, 0.38, 0.46, and 0.49 mW, respectively. The red line corresponds to the value of the heralded second-order auto-correlation $g^{(2)}(0) = 0.5$.

of 1 ns around each peak maximum.[51] This choice ensures that the coincidence window remains within the boundaries of the individual coincidence peaks, effectively excluding events that do not originate from our single-sided BFCs. Through the implementation of this approach, we are able to accumulate a sufficient number of coincidence counts, which provides us with reliable single-photon statistics. The minimum heralded $g^{(2)}(0) = 0.013 \pm 0.002$ is measured for the zeroth round trip at 0.25 mW pump power at a heralding rate of 20 kHz. For the first, second, third, and fourth cavity round trips, the minimum heralded $g^{(2)}(0)$ is measured to be 0.092 ± 0.002, 0.164 ± 0.002, 0.208 ± 0.003, and 0.465 ± 0.003 with 0.3, 0.34, 0.4, and 0.45 mW, respectively. At low pump powers, the observed $g^{(2)}(0)$ values for all cavity round trips remain below 0.5. This indicates single-photon state generation from our exponential-decay single-sided BFC. The value of heralded $g^{(2)}(0)$ exhibits proportionality to the pump power, which can be attributed to the Poisson statistics. The increase in minimum heralded $g^{(2)}(0)$ for multiple cavity round trips vs the zeroth cavity round trip is a result of the decreasing signal-to-noise ratio observed for those specific cross correlation peaks.

In Fig. 4(b), we present a summary of the HBT measurement results obtained using a time-reversed single-sided BFC. In this experimental configuration, we directed the unfiltered signal photons into an HBT auto-correlation measurement setup, which was heralded by the filtered idler photons. We use the same coincidence window of 1 ns around each correlation peak as in Fig. 4(a). The minimum heralded $g^{(2)}(0) = 0.016 \pm 0.002$ is measured for the zeroth round trip at 0.28 mW pump power with a heralding rate at 24 kHz. For the first, second, third, and fourth cavity round trips, the minimum heralded $g^{(2)}(0)$ is measured to be 0.115 ± 0.002, 0.207 ± 0.002, 0.247 ± 0.003, and 0.496 ± 0.003 with 0.33, 0.38, 0.46, and 0.49 mW, respectively. Our results are consistent with the exponential-decay singly filtered BFC in Fig. 4(a). For low pump powers, the heralded $g^{(2)}(0)$ values for all cavity round trips are smaller than 0.5, and heralded $g^{(2)}(0)$ is proportional to the pump power. The increase in minimum heralded $g^{(2)}(0)$ for multiple cavity round trips is due to the same rationale for the exponential-decay single-sided BFC. To further confirm the presence of multimode emission and single-photon anti-bunching characteristics in our time-reversible single-sided BFCs, we further obtain minimum heralded $g^{(2)}(0) = 0.204 \pm 0.002$, and $g^{(2)}(0) = 0.212 \pm 0.002$ by using a larger coincidence window of 30 ns to include the zeroth and first cavity round trips for both exponential-decay and time-reversed BFCs (see the supplementary material for more details). Our results indicate that the single-photon quantum nature is preserved in our time-reversed single-sided BFCs.

C. Comparison with other biphoton sources

After demonstrating completely resolvable and reversible of temporal envelopes in our single-sided BFCs, we proceed to compare our ultra-narrowband biphoton source with other studies in the literature. In Fig. 5, we present a summary of the cavity FSR and linewidth of selected cavity-enhanced SPDC sources and filtered BFCs, compared to our time-reversed ultra-narrowband biphoton source. The selected cavity-enhanced SPDCs and post-filtered BFCs include singly resonant,[26,40,43,48,49] singly filtered,[62] doubly resonant,[39,42,44,45,47,50,52–55,57] doubly filtered,[60] and triply resonant[46,51] configurations. The FSR is expressed in GHz, while

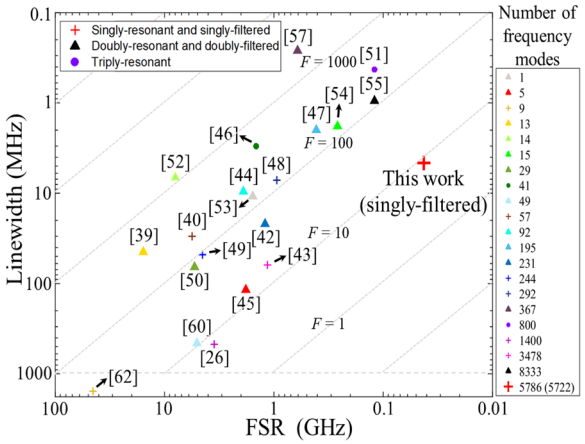

FIG. 5. Summary of FSR and linewidth of various biphoton sources. The figure-of-merits are FSR (GHz) and linewidth (MHz). The selected biphoton sources include singly resonant,[26,40,43,48,49] singly filtered,[62] doubly resonant,[39,42,44,45,47,50,52–55,57] doubly filtered,[60] and triply resonant[46,51] configurations. This work represents the narrowest FSR biphoton source to date, with the average number of frequency modes up to 5786 (and 5722). Furthermore, our source also exhibits the longest temporal coherence time of ≈217 ns among all the singly configured sources reported to date. These results highlight the advancements made in ultra-narrow FSR and dense-frequency mode numbers as well as an extended temporal coherence time in the biphoton sources. The gray dashed lines represent the different cavity finesse *F*.

the linewidth is measured in MHz. These parameters characterize the multimode quantum sources and highlight the improvements achieved in terms of FSR and linewidth in our time-reversed fully time-resolved biphoton source.

The typical bandwidth of EIT-based quantum memory ranges from 0.1 to 100 MHz,[30,31] and that of CRIB/GEM and AFC-based quantum memories lies between several MHz to 100 MHz.[17,28,29,32–36] Furthermore, the time-reversal characteristic of our biphoton sources may also be exploited to optimize the efficiency of storage and retrieval of photons in atomic quantum memories.[3,4,10,17,19] Hence, our time-reversed ultra-narrowband biphoton source can be compatible with these atomic quantum memory protocols. The present work has the narrowest FSR in a biphoton source, with an expected number of frequency modes reaching 5786 and 5722 (see the supplementary material for additional information). Furthermore, it has the longest coherence time of up to 217 ns among all the previously reported single-sided configurations. These results highlight the advancements of our biphoton sources made in terms of FSR, frequency mode count, and coherence time. These fully time-resolved multi-temporal modes can also be utilized for high-dimensional quantum information processing[54,55] or temporal-multiplexed quantum storage.[68] In addition, with the advancement of narrower bandwidth telecom frequency filters, or by using a cavity with a larger FSR,[60–62] it is also possible to implement frequency-multiplexed quantum storage[54] with dense frequency modes in our BFC sources.

Here, we also provide detailed discussions regarding the applicability and limitations of our method for potential applications. The post-filtered scheme has the flexibility to utilize cavities with different FSRs and linewidths. Typically, a smaller cavity FSR is better to encode more frequency modes given the fixed bandwidth of spontaneous parametric downconversion (SPDC) sources and to fully resolve temporal oscillations as performed in this work, but when considering the existing minimum bandwidth of telecom tunable filters (usually on the order of few GHz), this also limits the cavity FSR we can choose for frequency-bin encoding applications. Meanwhile, a larger cavity FSR (such as 50 GHz) is directly compatible with off-the-shelf multiplexing components; hence, it is more straightforward to implement frequency-bin encoding in this case; however, given the typical temporal resolution of single-photon detectors (on the order of dozens to hundreds of ps), such a temporal multimode feature cannot be detected easily. As for the cavity linewidth, given the fixed cavity FSR, a smaller linewidth corresponds to flatten temporal cross correlation and longer coherence time, while a larger linewidth leads to the opposite but with less filtering loss. Overall, we can summarize that our post-filtering schemes are robust and flexible without requiring a stabilization system nor a customized cavity design as required in cavity-enhanced SPDC sources, but the cavity-enhanced schemes can achieve higher source brightness without filtering. Finally, we note that the decreasing signal-to-noise ratio for temporal second-order cross correlation measurements (and JTI measurements) with multiple cavity round trips can be improved in the future by employing a cavity with higher finesse *F*, as confirmed in our prior work.[73]

III. CONCLUSION

In this work, we have demonstrated a time-reversible, fully time-resolved ultra-narrowband telecommunication biphoton source using single-sided BFCs. With the ultra-narrowband single-sided BFCs, we realized the reversed and fully time-resolved multimode oscillations without using frequency filters or specially designed cavities. We experimentally observe time-reversed and fully time-resolved second-order cross correlation and JTI measurements via our single-sided BFCs using only commercial single-photon detectors. Here, we point out that the time-reversibility of our source could be useful for enhancing the efficiency of quantum storage in atomic memories. The completely resolved temporal oscillations in our source provide a possible route to harness the temporal information in single-sided BFCs fully. Then, we verified that the multimode emission and single-photon state generation are preserved in our biphoton sources with HBT measurements. To the best of our knowledge, our biphoton source has the narrowest average FSR of ≈42.66 MHz and a linewidth of ≈4.6 MHz, resulting in a dense frequency mode number of 5786. In addition, our source exhibits the longest coherence time of 217 ns among all the previously reported singly configurations. These characteristics of our presented sources highlight the advancements in FSR, frequency mode count, and coherence time in the biphoton sources. Our time-reversed and fully time-resolved ultra-narrowband telecommunication biphoton source can be helpful for advanced quantum information processing tasks, such as high-dimensional time–frequency entanglement, and practical quantum applications, such as efficient multimode quantum storage toward long-distance and large-scale quantum networks.

SUPPLEMENTARY MATERIAL

The supplementary material contains information on the joint temporal intensity of exponential-decay and time-reversed single-sided BFCs. It also contains detailed information about FFPC used in this work, data of the heralded second-order auto-correlation function for time-reversible single-sided BFCs using a coincidence window of 30 ns, and the measured frequency spectrum of SPDC and the modeled frequency spectrum for time-reversible single-sided BFCs.

ACKNOWLEDGMENTS

The authors thank Vikas Anant for discussions on the superconducting nanowire single-photon detectors and Justin Caram for the help on the heralded auto-correlation measurements using a HydraHarp 400. This study was supported by the National Science Foundation under Award Nos. 1741707 (EFRI ACQUIRE), 1919355, 1936375 (QII-TAQS), and 2137984 (QuIC-TAQS) and the Army Research Office Multidisciplinary University Research Initiative (Grant No. W911NF-21-2-0214).

AUTHOR DECLARATIONS

Conflict of Interest

The authors have no conflicts to disclose.

Author Contributions

K.-C.C. and X.C. contributed equally to this paper.

K.-C.C. developed the idea and conducted the measurements. K.-C.C. and X.C. performed data analysis. K.-C.C., M.C.S., and X.C. contributed to the theory and numerical modeling. X.C. and C.W.W. supported and discussed the studies. K.-C.C., X.C., and C.W.W. prepared the manuscript. C.W.W. supervised the project. All authors contributed to the discussion and revision of the manuscript.

Kai-Chi Chang: Conceptualization (equal); Data curation (equal); Formal analysis (equal); Investigation (equal); Methodology (equal); Writing – original draft (equal); Writing – review & editing (equal). **Xiang Cheng**: Investigation (equal); Methodology (equal). **Murat Can Sarihan**: Investigation (equal); Methodology (equal); Software (equal). **Chee Wei Wong**: Supervision (equal); Writing – review & editing (equal).

DATA AVAILABILITY

The data that support the findings of this study are available from the corresponding author upon reasonable request.

REFERENCES

[1] G. Lerosey, J. De Rosny, A. Tourin, A. Derode, G. Montaldo, and M. Fink, "Time reversal of electromagnetic waves," Phys. Rev. Lett. **92**, 193904 (2004).
[2] M. F. Yanik and S. Fan, "Time reversal of light with linear optics and modulators," Phys. Rev. Lett. **93**, 173903 (2004).
[3] A. V. Gorshkov, A. André, M. Fleischhauer, A. S. Sørensen, and M. D. Lukin, "Universal approach to optimal photon storage in atomic media," Phys. Rev. Lett. **98**, 123601 (2007).
[4] I. Novikova, A. V. Gorshkov, D. F. Phillips, A. S. Sørensen, M. D. Lukin, and R. L. Walsworth, "Optimal control of light pulse storage and retrieval," Phys. Rev. Lett. **98**, 243602 (2007).
[5] G. Lerosey, J. De Rosny, A. Tourin, and M. Fink, "Focusing beyond the diffraction limit with far-field time reversal," Science **315**, 1120 (2007).
[6] I. M. Vellekoop, A. Lagendijk, and A. P. Mosk, "Exploiting disorder for perfect focusing," Nat. Photonics **4**, 320 (2010).
[7] Y. Sivan and J. B. Pendry, "Time reversal in dynamically tuned zero-gap periodic systems," Phys. Rev. Lett. **106**, 193902 (2011).
[8] W. Wan, Y. Chong, L. Ge, H. Noh, A. D. Stone, and H. Cao, "Time-reversed lasing and interferometric control of absorption," Science **331**, 889 (2011).
[9] A. P. Mosk, A. Lagendijk, G. Lerosey, and M. Fink, "Controlling waves in space and time for imaging and focusing in complex media," Nat. Photonics **6**, 283 (2012).
[10] S. A. Aljunid, G. Maslennikov, Y. Wang, H. L. Dao, V. Scarani, and C. Kurtsiefer, "Excitation of a single atom with exponentially rising light pulses," Phys. Rev. Lett. **111**, 103001 (2013).
[11] M. Bader, S. Heugel, A. L. Chekhov, M. Sondermann, and G. Leuchs, "Efficient coupling to an optical resonator by exploiting time-reversal symmetry," New J. Phys. **15**, 123008 (2013).
[12] V. Bacot, M. Labousse, A. Eddi, M. Fink, and E. Fort, "Time reversal and holography with spacetime transformations," Nat. Phys. **12**, 972 (2016).
[13] M. A. Gaafar, T. Baba, M. Eich, and A. Y. Petrov, "Front-induced transitions," Nat. Photonics **13**, 737 (2019).
[14] K. Pichler, M. Kühmayer, J. Böhm, A. Brandstötter, P. Ambichl, U. Kuhl, and S. Rotter, "Random anti-lasing through coherent perfect absorption in a disordered medium," Nature **567**, 351 (2019).
[15] D. Yang, S. H. Oh, J. Han, G. Son, J. Kim, J. Kim, M. Lee, and K. An, "Realization of superabsorption by time reversal of superradiance," Nat. Photonics **15**, 272 (2021).
[16] B. Swingle, G. Bentsen, M. Schleier-Smith, and P. Hayden, "Measuring the scrambling of quantum information," Phys. Rev. A **94**, 040302 (2016).
[17] G. Hetet, J. J. Longdell, A. L. Alexander, P. K. Lam, and M. J. Sellars, "Electro-optic quantum memory for light using two-level atoms," Phys. Rev. Lett. **100**, 023601 (2008).
[18] S. Ritter, C. Nölleke, C. Hahn, A. Reiserer, A. Neuzner, M. Uphoff, M. Mücke, E. Figueroa, J. Bochmann, and G. Rempe, "An elementary quantum network of single atoms in optical cavities," Nature **484**, 195 (2012).
[19] C. Liu, Y. Sun, L. Zhao, S. Zhang, M. M. T. Loy, and S. Du, "Efficiently loading a single photon into a single-sided Fabry–Perot cavity," Phys. Rev. Lett. **113**, 133601 (2014).
[20] B. Srivathsan, G. K. Gulati, A. Cere, B. Chng, and C. Kurtsiefer, "Reversing the temporal envelope of a heralded single photon using a cavity," Phys. Rev. Lett. **113**, 163601 (2014).
[21] J. Wenner, Y. Yin, Y. Chen, R. Barends, B. Chiaro, E. Jeffrey, J. Kelly, A. Megrant, J. Y. Mutus, C. Neill, P. J. J. O'Malley *et al.*, "Catching time-reversed microwave coherent state photons with 99.4% absorption efficiency," Phys. Rev. Lett. **112**, 210501 (2014).
[22] E. Flurin, N. Roch, J. D. Pillet, F. Mallet, and B. Huard, "Superconducting quantum node for entanglement and storage of microwave radiation," Phys. Rev. Lett. **114**, 090503 (2015).
[23] S. Gasparinetti, M. Pechal, J. C. Besse, M. Mondal, C. Eichler, and A. Wallraff, "Correlations and entanglement of microwave photons emitted in a cascade decay," Phys. Rev. Lett. **119**, 140504 (2017).
[24] P. Kurpiers, P. Magnard, T. Walter, B. Royer, M. Pechal, J. Heinsoo, Y. Salathé, A. Akin, S. Storz, J. C. Besse, S. Gasparinetti *et al.*, "Deterministic quantum state transfer and remote entanglement using microwave photons," Nature **558**, 264 (2018).
[25] P. Kurpiers, M. Pechal, B. Royer, P. Magnard, T. Walter, J. Heinsoo, Y. Salathé, A. Akin, S. Storz, J. C. Besse, S. Gasparinetti *et al.*, "Quantum communication with time-bin encoded microwave photons," Phys. Rev. Appl. **12**, 044067 (2019).

[26]R. Ikuta, R. Tani, M. Ishizaki, S. Miki, M. Yabuno, H. Terai, N. Imoto, and T. Yamamoto, "Frequency-multiplexed photon pairs over 1000 modes from a quadratic nonlinear optical waveguide resonator with a singly resonant configuration," Phys. Rev. Lett. **123**, 193603 (2019).
[27]K. Shinbrough, B. D. Hunt, and V. O. Lorenz, "Optimization of broadband Λ-type quantum memory using Gaussian pulses," Phys. Rev. A **103**, 062418 (2021).
[28]A. I. Lvovsky, B. C. Sanders, and W. Tittel, "Optical quantum memory," Nat. Photonics **3**, 706 (2009).
[29]N. Sangouard, C. Simon, H. De Riedmatten, and N. Gisin, "Quantum repeaters based on atomic ensembles and linear optics," Rev. Mod. Phys. **83**, 33 (2011).
[30]M. Fleischhauer and M. D. Lukin, "Dark-state polaritons in electromagnetically induced transparency," Phys. Rev. Lett. **84**, 5094 (2000).
[31]D. F. Phillips, A. Fleischhauer, A. Mair, R. L. Walsworth, and M. D. Lukin, "Storage of light in atomic vapor," Phys. Rev. Lett. **86**, 783 (2001).
[32]A. L. Alexander, J. J. Longdell, M. J. Sellars, and N. B. Manson, "Photon echoes produced by switching electric fields," Phys. Rev. Lett. **96**, 043602 (2006).
[33]N. Sangouard, C. Simon, M. Afzelius, and N. Gisin, "Analysis of a quantum memory for photons based on controlled reversible inhomogeneous broadening," Phys. Rev. A **75**, 032327 (2007).
[34]M. Afzelius, C. Simon, H. De Riedmatten, and N. Gisin, "Multimode quantum memory based on atomic frequency combs," Phys. Rev. A **79**, 052329 (2009).
[35]H. De Riedmatten, M. Afzelius, M. U. Staudt, C. Simon, and N. Gisin, "A solid-state light–matter interface at the single-photon level," Nature **456**, 773 (2008).
[36]L. Ma, O. Slattery, and X. Tang, "Optical quantum memory based on electromagnetically induced transparency," J. Opt. **19**, 043001 (2017).
[37]U. A. Javid, J. Ling, J. Staffa, M. Li, Y. He, and Q. Lin, "Ultrabroadband entangled photons on a nanophotonic chip," Phys. Rev. Lett. **127**, 183601 (2021).
[38]Y. Wang, K. D. Jöns, and Z. Sun, "Integrated photon-pair sources with nonlinear optics," Appl. Phys. Rev. **8**, 011314 (2021).
[39]Z. Y. Ou and Y. J. Lu, "Cavity enhanced spontaneous parametric down-conversion for the prolongation of correlation time between conjugate photons," Phys. Rev. Lett. **83**, 2556 (1999).
[40]C. E. Kuklewicz, E. Keskiner, F. N. C. Wong, and J. H. Shapiro, "A high-flux entanglement source based on a doubly resonant optical parametric amplifier," J. Opt. B: Quantum Semiclassical Opt. **4**, S162 (2002).
[41]H. Goto, Y. Yanagihara, H. Wang, T. Horikiri, and T. Kobayashi, "Observation of an oscillatory correlation function of multimode two-photon pairs," Phys. Rev. A **68**, 015803 (2003).
[42]C. E. Kuklewicz, F. N. C. Wong, and J. H. Shapiro, "Time-bin-modulated biphotons from cavity-enhanced down-conversion," Phys. Rev. Lett. **97**, 223601 (2006).
[43]M. Scholz, F. Wolfgramm, U. Herzog, and O. Benson, "Narrow-band single photons from a single-resonant optical parametric oscillator far below threshold," Appl. Phys. Lett. **91**, 191104 (2007).
[44]X. H. Bao, Y. Qian, J. Yang, H. Zhang, Z. B. Chen, T. Yang, and J. W. Pan, "Generation of narrow-band polarization-entangled photon pairs for atomic quantum memories," Phys. Rev. Lett. **101**, 190501 (2008).
[45]E. Pomarico, B. Sanguinetti, N. Gisin, R. Thew, H. Zbinden, G. Schreiber, A. Thomas, and W. Sohler, "Waveguide-based OPO source of entangled photon pairs," New J. Phys. **11**, 113042 (2009).
[46]M. Scholz, L. Koch, and O. Benson, "Statistics of narrow-band single photons for quantum memories generated by ultrabright cavity-enhanced parametric down-conversion," Phys. Rev. Lett. **102**, 063603 (2009).
[47]J. Fekete, D. Rieländer, M. Cristiani, and H. de Riedmatten, "Ultranarrow-band photon-pair source compatible with solid state quantum memories and telecommunication networks," Phys. Rev. Lett. **110**, 220502 (2013).
[48]A. Lenhard, M. Bock, C. Becher, S. Kucera, J. Brito, P. Eich, P. Müller, and J. Eschner, "Telecom-heralded single-photon absorption by a single atom," Phys. Rev. A **92**, 063827 (2015).
[49]O. Slattery, L. Ma, P. Kuo, and X. Tang, "Narrow-linewidth source of greatly non-degenerate photon pairs for quantum repeaters from a short singly resonant cavity," Appl. Phys. B **121**, 413 (2015).
[50]K. H. Luo, H. Herrmann, S. Krapick, B. Brecht, R. Ricken, V. Quiring, H. Suche, W. Sohler, and C. Silberhorn, "Direct generation of genuine single-longitudinal-mode narrowband photon pairs," New J. Phys. **17**, 073039 (2015).
[51]M. Rambach, A. Nikolova, T. J. Weinhold, and A. G. White, "Sub-megahertz linewidth single photon source," APL Photonics **1**, 096101 (2016).
[52]P. J. Tsai and Y. C. Chen, "Ultrabright, narrow-band photon-pair source for atomic quantum memories," Quantum Sci. Technol. **3**, 034005 (2018).
[53]A. Moqanaki, F. Massa, and P. Walther, "Novel single-mode narrow-band photon source of high brightness tuned to cesium D2 line," APL Photonics **4**, 090804 (2019).
[54]A. Seri, D. Lago-Rivera, A. Lenhard, G. Corrielli, R. Osellame, M. Mazzera, and H. de Riedmatten, "Quantum storage of frequency-multiplexed heralded single photons," Phys. Rev. Lett. **123**, 080502 (2019).
[55]K. Niizeki, D. Yoshida, K. Ito, I. Nakamura, N. Takei, K. Okamura, M. Y. Zheng, X. P. Xie, and T. Horikiri, "Two-photon comb with wavelength conversion and 20-km distribution for quantum communication," Commun. Phys. **3**, 138 (2020).
[56]K. Ito, T. Kondo, K. Mannami, K. Niizeki, D. Yoshida, K. Minaguchi, M. Zheng, X. Xie, F. L. Hong, and T. Horikiri, "Frequency-multiplexed storage and distribution of narrowband telecom photon pairs over a 10-km fiber link with long-term system stability," Phys. Rev. Appl. **19**, 024070 (2023).
[57]J. Liu, J. Liu, P. Yu, and G. Zhang, "Sub-megahertz narrow-band photon pairs at 606 nm for solid-state quantum memories," APL Photonics **5**, 066105 (2020).
[58]Y. J. Lu, R. L. Campbell, and Z. Y. Ou, "Mode-locked two-photon states," Phys. Rev. Lett. **91**, 163602 (2003).
[59]Z. Xie, T. Zhong, S. Shrestha, X. Xu, J. Liang, Y. X. Gong, J. C. Bienfang, A. Restelli, J. H. Shapiro, F. N. C. Wong, and C. Wei Wong, "Harnessing high-dimensional hyperentanglement through a biphoton frequency comb," Nat. Photonics **9**, 536 (2015).
[60]K.-C. Chang, X. Cheng, M. C. Sarihan, A. K. Vinod, Y. S. Lee, T. Zhong, Y. X. Gong, Z. Xie, J. H. Shapiro, F. N. C. Wong, and C. W. Wong, "648 Hilbert-space dimensionality in a biphoton frequency comb: Entanglement of formation and Schmidt mode decomposition," npj Quantum Inf. **7**, 48 (2021).
[61]K.-C. Chang, X. Cheng, M. C. Sarihan, F. N. C. Wong, J. H. Shapiro, and C. W. Wong, "High-dimensional energy-time entanglement distribution via a biphoton frequency comb," in *Conference on Lasers and Electro-Optics, OSA Technical Digest* (Optical Society of America, 2021), p. FF1A.7.
[62]X. Cheng, K.-C. Chang, M. C. Sarihan, A. Mueller, M. Spiropulu, M. D. Shaw, B. A. Korzh, A. Faraon, F. N. C. Wong, J. H. Shapiro, and C. W. Wong, "High-dimensional time-frequency entanglement in a singly-filtered biphoton frequency comb," Commun. Phys. **6**, 278 (2023).
[63]C. Reimer, M. Kues, P. Roztocki, B. Wetzel, F. Grazioso, B. E. Little, S. T. Chu, T. Johnston, Y. Bromberg, L. Caspani, D. J. Moss, and R. Morandotti, "Generation of multiphoton entangled quantum states by means of integrated frequency combs," Science **351**, 1176 (2016).
[64]J. A. Jaramillo-Villegas, P. Imany, O. D. Odele, D. E. Leaird, Z. Y. Ou, M. Qi, and A. M. Weiner, "Persistent energy-time entanglement covering multiple resonances of an on-chip biphoton frequency comb," Optica **4**, 655 (2017).
[65]M. Kues, C. Reimer, J. M. Lukens, W. J. Munro, A. M. Weiner, D. J. Moss, and R. Morandotti, "Quantum optical microcombs," Nat. Photonics **13**, 170 (2019).
[66]I. Craiciu, M. Lei, J. Rochman, J. M. Kindem, J. G. Bartholomew, E. Miyazono, T. Zhong, N. Sinclair, and A. Faraon, "Nanophotonic quantum storage at telecommunication wavelength," Phys. Rev. Appl. **12**, 024062 (2019).
[67]I. Craiciu, M. Lei, J. Rochman, J. G. Bartholomew, and A. Faraon, "Multifunctional on-chip storage at telecommunication wavelength for quantum networks," Optica **8**, 114 (2021).
[68]A. Tiranov, S. Designolle, E. Z. Cruzeiro, J. Lavoie, N. Brunner, M. Afzelius, M. Huber, and N. Gisin, "Quantification of multidimensional entanglement stored in a crystal," Phys. Rev. A **96**, 040303 (2017).
[69]U. Herzog, M. Scholz, and O. Benson, "Theory of biphoton generation in a single-resonant optical parametric oscillator far below threshold," Phys. Rev. A **77**, 023826 (2008).
[70]J. P. W. MacLean, J. M. Donohue, and K. J. Resch, "Direct characterization of ultrafast energy-time entangled photon pairs," Phys. Rev. Lett. **120**, 053601 (2018).

[71] S. Mittal, V. V. Orre, A. Restelli, R. Salem, E. A. Goldschmidt, and M. Hafezi, "Temporal and spectral manipulations of correlated photons using a time lens," Phys. Rev. A **96**, 043807 (2017).
[72] B. Korzh, Q. Y. Zhao, J. P. Allmaras, S. Frasca, T. M. Autry, E. A. Bersin, A. D. Beyer, R. M. Briggs, B. Bumble, M. Colangelo, G. M. Crouch, A. E. Dane, T. Gerrits, A. E. Lita, F. Marsili, G. Moody, C. Peña, E. Ramirez, J. D. Rezac, N. Sinclair, M. J. Stevens, A. E. Velasco, V. B. Verma, E. E. Wollman, S. Xie, D. Zhu, P. D. Hale, M. Spiropulu, K. L. Silverman, R. P. Mirin, S. W. Nam, A. G. Kozorezov, M. D. Shaw, and K. K. Berggren, "Demonstration of sub-3 ps temporal resolution with a superconducting nanowire single-photon detector," Nat. Photonics **14**, 250 (2020).
[73] K.-C. Chang, X. Cheng, M. C. Sarihan, and C. W. Wong, "Towards optimum Franson interference recurrence in mode-locked singly-filtered biphoton frequency combs," Photonics Res. **11**, 1175 (2023).

Supplementary Material:

Time-reversible and fully time-resolved ultranarrow-band biphoton frequency combs

Kai-Chi Chang[1,2,*], Xiang Cheng[1,2,*], Murat Can Sarihan[1], and Chee Wei Wong[1,*]

[1]Fang Lu Mesoscopic Optics and Quantum Electronics Laboratory, Department of Electrical and Computer Engineering, University of California, Los Angeles, CA 90095, USA

[2]These authors contributed equally to this work.

*Emails: uclakcchang@g.ucla.edu; chengxiang@g.ucla.edu; cheewei.wong@g.ucla.edu

I. Joint temporal intensity of the exponential-decay and time-reversed single-sided BFCs

Based on Eqs. (1) to (3) in the main text, here we derive the joint temporal intensity (JTI) of the exponential-decay and time-reversed single-sided biphoton frequency combs (BFCs) [1], which can be written as follows:

$$K^{cross}_{exponential-decay}(t_I - t_S) = \int_{-\infty}^{\infty} \frac{d\omega}{2\pi} \frac{i\sqrt{N_S}\mathrm{sinc}(\omega t_{\mathrm{coh}}/2)e^{-4\omega^2 ln(2)/\Delta\omega^2} e^{i\omega(t_I - t_S - t_{\mathrm{coh}}/2)}}{1+i\frac{\Delta\Omega}{\pi\Delta\omega} sin(\pi\omega/\Delta\Omega)e^{-i\pi\omega/\Delta\Omega}}, \quad (1)$$

and

$$K^{cross}_{time-reversed}(t_I - t_S) = \int_{-\infty}^{\infty} \frac{d\omega}{2\pi} \frac{i\sqrt{N_S}\mathrm{sinc}(\omega t_{\mathrm{coh}}/2)e^{-4\omega^2 ln(2)/\Delta\omega^2} e^{i\omega(t_S - t_I - t_{\mathrm{coh}}/2)}}{1+i\frac{\Delta\Omega}{\pi\Delta\omega} sin(\pi\omega/\Delta\Omega)e^{-i\pi\omega/\Delta\Omega}}, \quad (2)$$

respectively. Here, N_S is the source brightness; $t_{\mathrm{coh}} = 3.54$ ps is the coherence time of our spontaneous parametric down-conversion (SPDC) source; $\Delta\omega/2\pi$ is the bandwidth of tunable bandpass filter (BPF). We can understand the reversing of temporal oscillations (or equivalently, JTI) of our singly-filtered BFCs originates from the swapping of a fiber Fabry-Perot cavity (FFPC) between the signal and idler channels.

II. Detailed information about the ultranarrow FFPC

Here we provide detailed information about the FFPC used in this work. In Figure 1(a), we provide the detailed cross section of a standard FFPC (provide from Luna Innovations), and the length of fiber basically corresponds to the cavity length. Figure 1(b) is the actual device illustration before we mount it with our custom-made double-temperature shielding layers. Then, we summarized the specifications of this FFPC as follows: 1. The calculated cavity length for FFPC used in this work is 2.04 m. 2. The input/output mirrors have a reflectivity of approximately 90%. 3. The wavelength range is 1520 to 1620 nm. 4. Thermal coefficient is calculated as ≈ 1.6 GHz/°C. Hence, our custom-made double-temperature shielding layers can provide a temperature control stability of approximately 1.6 MHz (≈ 1 mK) over 24-hours. 5. The insertion loss of this device is measured to be 0.55 dB at 1570 nm.

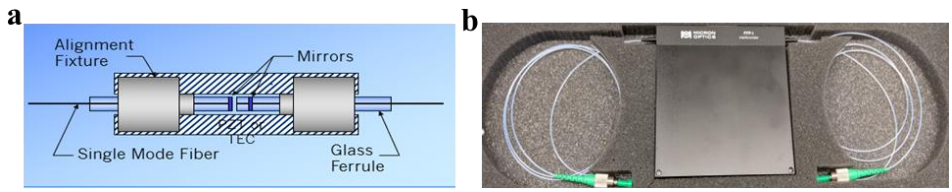

Figure 1. Detailed illustration of the FFPC. (a) The cross section of an example internal structure of a FFPC. (b) The illustration of the actual device package before mounting and stabilizing its temperature.

III. Measured heralded second-order auto-correlation function for time-reversible single-sided BFCs using a coincidence window of 30 ns

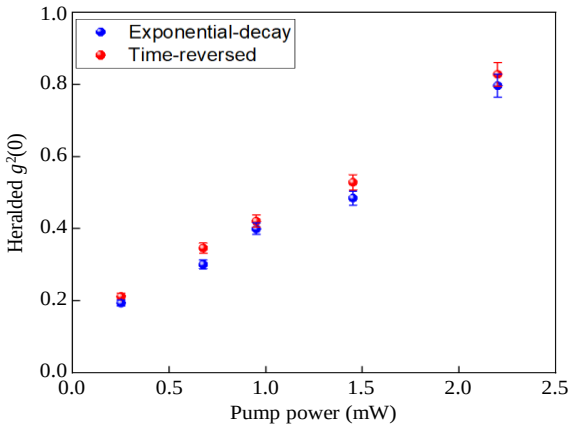

Figure 2. Measured heralded second-order auto-correlation function $g^{(2)}(0)$ versus the pump power for exponential-decay and time-reversed 42 MHz single-sided BFCs using a 30 ns coincidence window. HBT measurements for time-reversible singly-filtered BFCs. The minimum heralded $g^{(2)}(0) = 0.204 \pm 0.002$ and $g^{(2)}(0) = 0.212 \pm 0.002$ is measured using a wider coincidence window of 30 ns, which includes 0^{th} and 1^{st} cavity round-trip correlation peaks from both exponential-decay and time-reversed single-sided BFCs.

In this section, we provide the heralded second-order auto-correlation function measurements using a coincidence window of 30 ns for time-reversible single-sided BFCs, as given in Figure 2. The main difference between these results and those in main text Figure 4 is the chosen coincidence window. Here, we use a larger coincidence window of 30 ns to cover the 0^{th} and 1^{st} cavity round-trip correlation peaks from both exponential-decay and time-reversed singly-filtered BFCs to verify its multimode emission. For both measurements, similar to in the main text, we send the unfiltered idler and signal photons into Hanbury Brown and Twiss (HBT) interferometer while the filtered signal and idler photons are used as heralding.

Similar to previous narrow-band biphoton sources [2, 3], we achieve minimum heralded $g^{(2)}(0) = 0.204 \pm 0.002$, and $g^{(2)}(0) = 0.212 \pm 0.002$ for time-reversible single-sided BFCs, and the values of measured heralded $g^{(2)}(0)$ follow the similar trend versus pump power, which is consistent with our results in main text Figure 4. The non-ideal heralded $g^{(2)}(0)$ come from the decreasing signal-to-noise ratio when the width of the coincidence window 30 ns is much larger than the completely resolved correlation peak full-width-at-half-maximum (FWHM) (average value is ≈ 155.35 ps, from main text Figure 2 and Figure 3), majority of the accidental photons are included for heralded $g^{(2)}(0)$ measurements. Despite this limitation, we still observe single-photon statistics and confirm our time-reversible singly-filtered BFCs are multimode quantum sources.

IV. Measured frequency spectrum of spontaneous parametric down-conversion and modeled frequency spectrum for time-reversible single-sided BFCs

In this section, we present the experimental results to calibrate both signal and idler photons of our SPDC source using a telecom-band tunable BPF with FWHM of 0.3 nm. We first connect this BPF to signal photons while idler photons are directed to the single-photon detector for heralded coincidence measurements. Then, we switch the BPF to idler photons when signal photons are unfiltered. This method can be used to map out the wavelength of signal and idler photons, respectively.

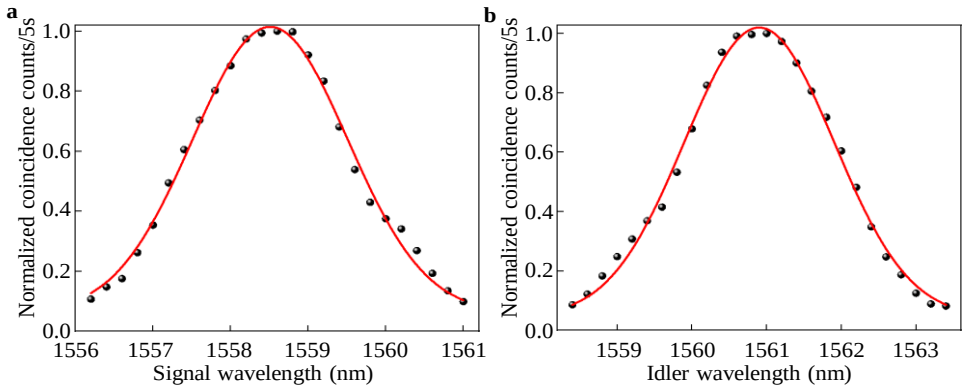

Figure 3. Measured SPDC spectrums of signal and idler photons. (a) Frequency spectrum of signal photons of the SPDC source used in this work. (b) Measured frequency spectrum of idler photons of the same biphoton source. The measurements are done by a telecom-band tunable Gaussian BPF with a FWHM bandwidth of 0.3 nm. Our SPDC source has a FWHM bandwidth of ≈ 247 GHz with ≈ 2.4 nm center wavelength difference.

Our results are shown in Figure 3(a) and 3(b), the center wavelengths of the signal and idler photon are at 1558.5 and 1560.9 nm, respectively. The bandwidth for signal and idler photons are measured to be ≈ 246.83, and ≈ 246.30 GHz, respectively. Next, by using the parameters of our SPDC source measured in Figure 3, we theoretically model the frequency spectrum of time-reversible singly-filtered BFCs. Figures 4(a) and 4(b) are the calculated single-sided BFC FWHM spectrum for signal and idler photons using a FFPC with average free-spectral range (FSR) of ≈ 42.66 MHz and ≈ 42.67 MHz, respectively. To the best of our knowledge, these FSR are the narrowest reported FSR up to date [1-23]. In Figure 4(c) and 4(d), we model the zoom-in singly-filtered BFC spectrum within the range of 0.02 nm at the center of SPDC spectrum to clearly resolve the discretized single-sided BFC spectrum. From the near-degenerate spectrum of SPDC photons and narrow FSR cavity, our time-reversible singly-filtered BFCs are thus expected to have a record high average number of frequency modes of 5,786 and 5,772 among all the reported single-sided BFC sources so far [1, 7, 10, 14, 15, 23]. The results are consistent with Eqs. (1) in the main text, our time-reversible singly-filtered BFCs have near-identical frequency spectrums due to their same joint spectral intensity (JSI) under different JTIs.

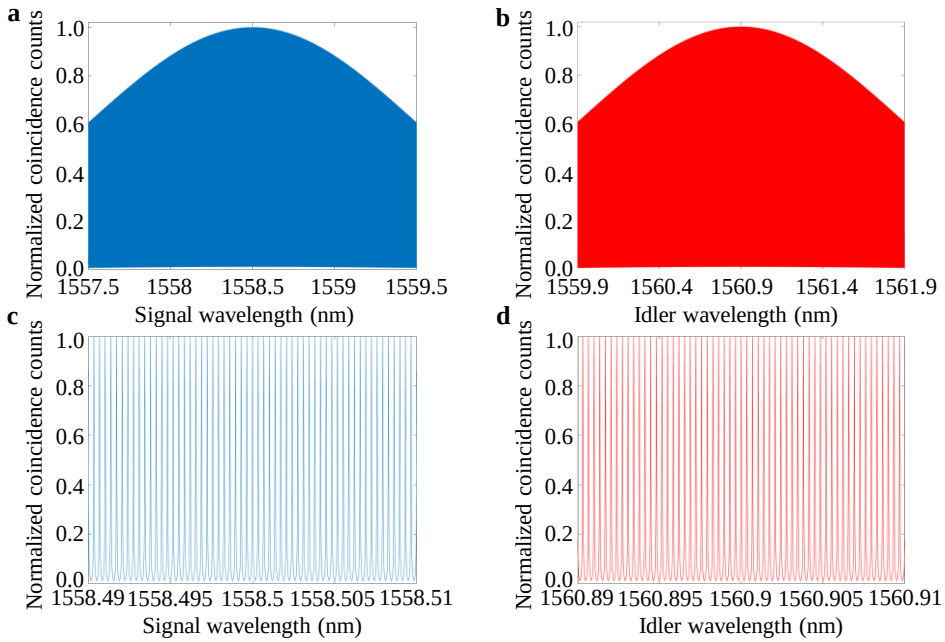

Figure 4. Modeled frequency spectrum of time-reversible 42.7 MHz single-sided BFCs. (a) and (b) Theoretical frequency spectrum of exponential-decay and time-reversed singly-filtered BFCs based on the wavelength calibration measurements from Figure 3. Figures 4(c) and 4(d) are the modeled zoom-in spectrum, which shows discretized spectrums for time-reversible single-sided BFCs. Combining the measured SPDC spectrum in Figure 3 with fully time-resolved JTIs from main text Figure 2 and Figure 3,

we expect our ultranarrow-band source has 5,786 and 5,772 frequency modes within the phase-matching bandwidth of the signal and idler photons.

References

[1] R. Ikuta, R. Tani, M. Ishizaki, S. Miki, M. Yabuno, H. Terai, N. Imoto, and T. Yamamoto, Frequency-multiplexed photon pairs over 1000 modes from a quadratic nonlinear optical waveguide resonator with a singly resonant configuration, *Phys. Rev. Lett.* **123**, 193603 (2019).

[2] M. Scholz, L. Koch, and O. Benson, Statistics of narrow-band single photons for quantum memories generated by ultrabright cavity-enhanced parametric down-conversion, *Phys. Rev. Lett.* **102**, 063603 (2009).

[3] M. Rambach, A. Nikolova, T. J. Weinhold, and A. G. White, Sub-megahertz linewidth single photon source, *APL Photon.* **1**, 096101 (2016).

[4] T. Zhong, F. N. C. Wong, T. D. Roberts, and P. Battle, High performance photon-pair source based on a fiber-coupled periodically poled KTiOPO4 waveguide, *Opt. Express* **17**, 12019 (2009).

[5] K.-C. Chang, X. Cheng, M. C. Sarihan, A. K. Vinod, Y. S. Lee, T. Zhong, Y. X. Gong, Z. Xie, J. H. Shapiro, F. N. C. Wong, and C. W. Wong, 648 Hilbert Space Dimensionality in a Biphoton Frequency Comb: entanglement of formation and Schmidt mode decomposition, *npj Quan. Inf.* **7**, 48 (2021).

[6] Z. Y. Ou, and Y. J. Lu, Cavity enhanced spontaneous parametric down-conversion for the prolongation of correlation time between conjugate photons, *Phys. Rev. Lett.* **83**, 2556 (1999).

[7] C. E. Kuklewicz, E. Keskiner, F. N. C. Wong, and J. H. Shapiro, A high-flux entanglement source based on a doubly resonant optical parametric amplifier, *J. Opt. Soc. Am. B* **4**, S162 (2002).

[8] Y. J. Lu, R. L. Campbell, and Z. Y. Ou, Mode-locked two-photon states, *Phys. Rev. Lett.* **91**, 163602 (2003).

[9] C. E. Kuklewicz, F. N. C. Wong, and J. H. Shapiro, Time-bin-modulated biphotons from cavity-enhanced down-conversion, *Phys. Rev. Lett.* **97**, 223601 (2006).

[10] M. Scholz, F. Wolfgramm, U. Herzog, and O. Benson, Narrow-band single photons from a single-resonant optical parametric oscillator far below threshold, *Appl. Phys. Lett.* **91**, 191104 (2007).

[11] X. H. Bao, Y. Qian, J. Yang, H. Zhang, Z. B. Chen, T. Yang, and J. W. Pan, Generation of narrow-band polarization-entangled photon pairs for atomic quantum memories, *Phys. Rev. Lett.* **101**, 190501 (2008).

[12] E. Pomarico, B. Sanguinetti, N. Gisin, R. Thew, H. Zbinden, G. Schreiber, A. Thomas, and W. Sohler, Waveguide-based OPO source of entangled photon pairs, *New J. Phys.* **11**, 113042 (2009).

[13] J. Fekete, D. Rieländer, M. Cristiani, and H. de Riedmatten, Ultranarrow-band photon-pair source compatible with solid state quantum memories and telecommunication networks, *Phys. Rev. Lett.* **110**, 220502 (2013).

[14] A. Lenhard, M. Bock, C. Becher, S. Kucera, J. Brito, P. Eich, P. Müller, and J. Eschner, Telecom-heralded single-photon absorption by a single atom, *Phys. Rev. A* **92**, 063827 (2015).

[S15] O. Slattery, L. Ma, P. Kuo, and X. Tang, Narrow-linewidth source of greatly non-degenerate photon pairs for quantum repeaters from a short singly resonant cavity, *Appl. Phys. B* **121**, 413 (2015).

[S16] K. H. Luo, H. Herrmann, S. Krapick, B. Brecht, R. Ricken, V. Quiring, H. Suche, W. Sohler, and C. Silberhorn, Direct generation of genuine single-longitudinal-mode narrowband photon pairs, *New J. Phys.* **17**, 073039 (2015).

[17] Z. Xie, T. Zhong, S. Shrestha, X. Xu, J. Liang, Y. X. Gong, J. C. Bienfang, A. Restelli, J. H. Shapiro, F. N. C. Wong, and C. W. Wong, Harnessing high-dimensional hyperentanglement through a biphoton frequency comb, *Nat. Photon.* **9**, 536 (2015).

[18] P. J. Tsai, and Y. C. Chen, Ultrabright, narrow-band photon-pair source for atomic quantum memories, *Quan. Sci. Technol.* **3**, 034005 (2018).

[19] A. Moqanaki, F. Massa, and P. Walther, Novel single-mode narrow-band photon source of high brightness tuned to cesium d2 line, *APL Photon.* **4**, 090804 (2019).

[20] A. Seri, D. Lago-Rivera, A. Lenhard, G. Corrielli, R. Osellame, M. Mazzera, and H. de Riedmatten, Quantum storage of frequency-multiplexed heralded single photons, *Phys. Rev. Lett.* **123**, 080502 (2019).

[21] K. Niizeki, D. Yoshida, K. Ito, I. Nakamura, N. Takei, K. Okamura, M. Y. Zheng, X. P. Xie, and T. Horikiri, Two-photon comb with wavelength conversion and 20-km distribution for quantum communication, *Commun. Phys.* **3**, 138 (2020).

[22] J. Liu, J. Liu, P. Yu, and G. Zhang, Sub-megahertz narrow-band photon pairs at 606 nm for solid-state quantum memories, *APL Photon.* **5**, 066105 (2020).

[23] K.-C. Chang, X. Cheng, M. C. Sarihan, F. N. C. Wong, J. H. Shapiro, and C. W. Wong, High-dimensional Energy-time Entanglement Distribution via a Biphoton Frequency Comb, in Conference on Lasers and Electro-Optics, OSA Technical Digest (Optical Society of America, 2021), paper FF1A.7.